Breaking of rod-shaped model material during compression

Kulaviak Lukas[1,*], *Penkavova* Vera[1], *Ruzicka* Marek[1], *Puncochar* Miroslav[1], *Zamostny* Petr[2], *Grof* Zdenek[3], *Stepanek* Frantisek[3], *Schongut* Marek[3], and *Havlica* Jaromir[1]

[1] Czech Academy of Science , Institute of Chemical Process Fundamentals, 16502 Rozvojova 2/135, Prague, Czech Republic
[2] University of Chemistry and Technology Prague, Department of Organic Technology, 16500 Technicka 5, Prague, Czech Republic
[3] University of Chemistry and Technology Prague, Department of Chemical Engineering, 16500 Technicka 3, Prague, Czech Republic

Abstract. The breakage of a model anisometric dry granular material caused by uniaxial compression was studied. The bed of uniform rod-like pasta particles (8 mm long, aspect ratio 1:8) was compressed (Gamlen Tablet Press) and their size distribution was measured after each run (Dynamic Image Analysing). The compression dynamics was recorded and the effect of several parameters was tested (rate of compression, volume of granular bed, pressure magnitude and mode of application). Besides the experiments, numerical modelling of the compressed breakable material was performed as well, employing the DEM approach (Discrete Element Method). The comparison between the data and the model looks promising.

1 Introduction

Anisometric granular particles commonly occur in many different materials and products (e.g. crystals, pharmaceutical ingredients, [1-2]). Many technological operations (filtration, washing, drying, transportation) can lead to uncontrolled changes in grain size distribution caused by attrition and breakage [3]. When a randomly packed bed of anisometric particles is compressed, either by its own weight or by an external force, the task is to find the relationship between the applied stress and the grain compressibility and breakage. The goal of this study is to experimentally measure the breakage dynamics, find some quantitative descriptive variables and estimate their values, as they depend on few important control parameters. Such an effort is of both scientific and application interest. The experimental data are used to validate numerical modelling of granular beds [4], as is also briefly shown in this study.

2 Experimental

2.1 Material properties

Based on the preliminary tests, the rod-shaped pasta was used as the model granular material. Cylindrical dry noodles Capellini Major (Italy) 26 cm long of diameter 1.06±0.02 mm were cut into 8 mm particles with multifunction tool DREMEL® 4200. The bundle of noodles, tightly constricted by a thermo-sensitive sleeve, was cut with a high-speed rotating (up to 35 000 rev. per min) thin (0.75 mm) diamond cutting disc (type SC545). The cut particles had a narrow size distribution and for the purpose of our experiments were considered as monodisperse (mean length 8 mm, standard deviations $1\sigma_{68\%}$ = 0.25 mm, $2\sigma_{95\%}$ = 0.65 mm). Their mechanical material properties were determined by the three point rigidity test using Brookfield CT3 Texture analyser with the following result: the elastic modulus is 4.9 GPa, stiffness 292 kN/m, bending modulus 5.67 mNm and bending stress 57.9 MPa.

2.2 Apparatus and methodology

2.1.1 Compression

The material was subjected to the uniaxial compression tests (force-displacement analysis) carried out in the apparatus GTP-1 (recently labelled as Gamlen R-Series, Gamlen Tableting Ltd.), which is capable to generate load up to 500 kg. We used 3 cylindrical stainless steel measuring cells with height 30 mm and of diameters D = 25, 33, 41 mm, referred to as: S (small), M (medium), L (large). The maximum reachable pressure in the small cell was 10 MPa. Several metal disk-shaped spacers were employed to adjust the initial height of the particles layer to three values: H = 10, 15, 20 mm. The initial volume V of particles was put in the cell manually, by pouring through a funnel. Piston speed v and applied load P were set and the measurement started. The piston moved downward at a constant speed and its position and the bed resistance force were measured at the sampling rate 200 Hz, till the value of P was reached. From the piston position, the actual bed volume was obtained and the compressibility calculated $C = \Delta V/V$, usually is shown in %. The typical reproducibility of the results from five measurements in terms of the standard deviation is 5%. The result was the dependence $C(P)$ shown in diagrams known as compressibility curves.

* Corresponding author: kulaviak@icpf.cas.cz

After reaching the terminal pre-set pressure P and the corresponding final compression, the piston returned to its initial position and the layer slightly relaxed due to the elastic relieve. Two modes of the applied pressure were tested: (i) single-run and (ii) repetitive. In the non-recurring mode, after the compression, the particles were taken out of the measuring cell for granulometry. In the recurring mode, after granulometry, the particles returned to the cell for the next run with the same pressure P.

2.1.2 Granulometry

The particle size distribution (PSD) of the grains before and after the compression tests was measured by the dry granulometry device (Solids particle size analyser, CANTY, Industrial SolidSizer). An ensemble of particles (typically 2000) passed through the vibratory conveyor forming a slowly moving mono-layer. It slid along the inclined plane to ensure 2D motion of the particles in front of the black&white camera (320 x 240 pxls, 5 fps). The particle images were analysed by the device software. Each 2D image of a particle was fitted inside enclosing rectangle whose major size was the particle length. The histograms of particle sizes were produced, using 200 regular bins. From this, 4 coarse bins were also made that are used here: B1 (1-3 mm), B2 (3-5 mm), B3 (5-7 mm), B4 (7-8 mm). The average length of particles L and distribution of particle length characterized by polydispersity Z were calculated from the individual moments $\mu_n = \sum_{j=1}^{P} l_j^n$ as:

$$L = \frac{\mu_1}{\mu_0}, \quad (1)$$

$$Z = \frac{\mu_0 \cdot \mu_2}{\mu_1^2}, \quad (2)$$

where P is the number of particles, j is the current particle index (j = 1, 2, ... P), l_j is the length of particle j, l_j^n is the n-th power of l_j, μ_n is the n-th moment.

2.1.3 Modelling

Computer simulation was employed, using the DEM approach (Discrete Element Method), to better understand the breakage mechanism whose results were observed in the experiments. The multi-element particle model was used [5]. The model details are present in [4, 6]. The model particle is a row of 21 partially overlapping rigid spherical elements connected by bonds that break when shear force or bending torque exceed a pre-set threshold. Selected modelling results regarding the pressure effects are shown in Sections 3.3 and 3.4, for demonstration.

3 Results and discussion

3.1 Rate of granular bed compression

The measuring cell M was used with the bed height H = 15 mm. The applied pressure was P = 5200 kPa. Six different compression rates were employed within the measuring range of the device: v = 0.1, 0.5, 1, 5, 10 and 60 mm/min. The result is shown in Fig. 1, where no apparent effect of the piston speed can be observed. Based on this, the medium piston speed v = 5 mm/min was used for the further tests.

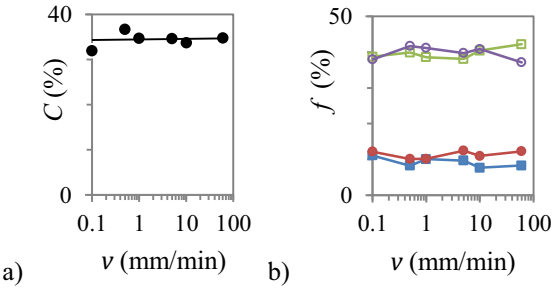

Fig. 1. Effect of compression rate v. (a) Compressibility C. (b) Particle fractions f in coarse bins: B4 - blue filled squares, B3 - red filled circles, B2 - green empty squares, B1 - purple empty circles. Applied pressure P = 5200 kPa.

3.2 Volume of granular bed

The initial volume of the compressed bed was adjusted by combining three cell sizes and three bed heights (9 combinations). Each measurement was repeated 5x and the results were averaged. The applied pressure was P = 3350 kPa. The result is shown in Fig. 2. The final compressibility in cells S and M is almost identical, and is slightly lower in cell L. The coarse bins' populations are not much influenced too. Thus the wall effects in our experiments were likely similar, in all cases. The medium cell size M and the middle layer height H = 15 mm were used for the further tests.

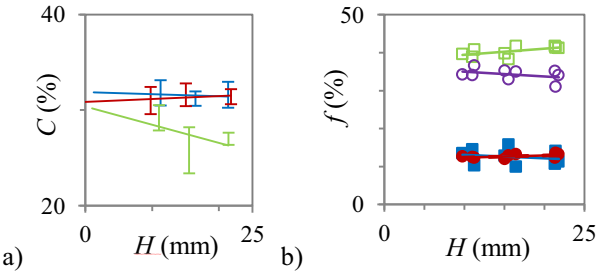

Fig. 2. Effect of bed volume. (a) Compressibility C; blue, red, green line for cells S, M, L. (b) Particle fractions f in coarse bins: B4 - blue filled squares, B3 - red filled circles, B2 - green empty squares, B1 - purple empty circles. Three marks at one H are 3 different cells. Applied pressure P = 3350 kPa.

3.3 Pressure magnitude

The effect of one-time applied pressure (non-repetitive) was tested, for eight values, P = 100, 500, 1000, 1400, 1900, 2600, 3350, 5200 kPa. The cell size was M and the layer height was H = 15 mm. The result is shown in Fig. 3. The shape of $C(P)$ graph obeys the typical saturation curve (3a), for both the data and model. At the load of 500 kPa, the particles break preferentially in half (green curve). At higher loads, the particles break into smaller pieces and progressively populate the size bins B1 and B2 (3b). The mean particle size is reduced by a high enough pressure, both in the data and model, Fig. 4. The wave-like course of the polydispersity is seen in Fig. 5.

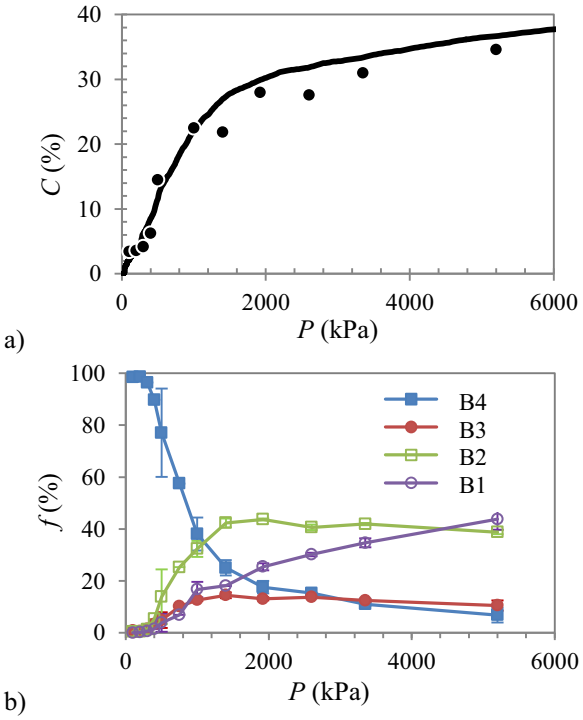

Fig. 3. Effect of applied pressure P (single compression). (a) Compressibility C; data - marks, model - line. (b) Particle fractions f in coarse bins B1-B4.

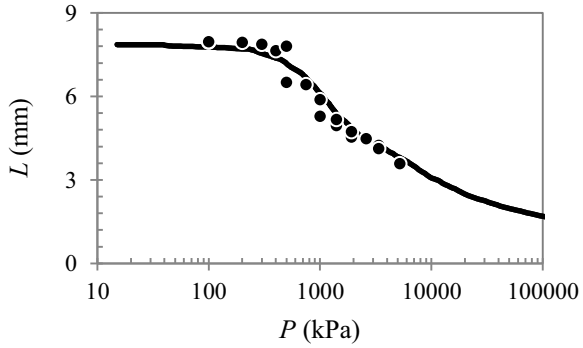

Fig. 4. Effect of applied pressure P (single compression) on particle average length, L; data – marks, model - line.

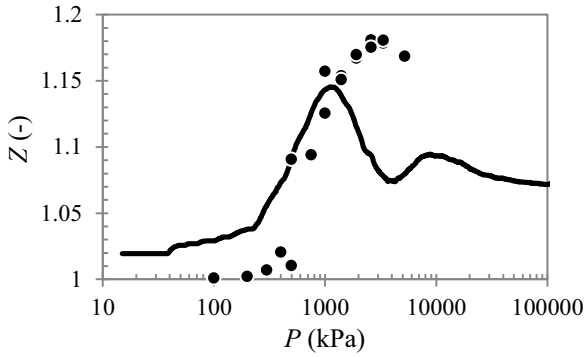

Fig. 5. Effect of applied pressure P (single compression) on particle polydispersity Z; data – marks, model - line.

3.4 Repeated compression

The relation between single and multiple compressions was studied too. The cell size was M and the layer height was 15 mm. The applied pressure P was set to 500 or 3350 kPa. The variable parameter was the number N = 1, 2, 3, 4, 5, of how many times the layer was consequently compressed, after emptying and re-filling the cell. The result is shown in Fig. 6. The $C(N)$ graphs are similar for both applied pressures (6a): weak almost linear rise over the limited range of N. The size distribution (6b) shows enhanced destruction of the particles, as compared with that in Fig. 3b. After two runs (N = 2), the initial length (bin B4) is missing and the population in the half-size bin (B2) stops growing. With more runs, the small particles (B1) grow in number at the expense of the others, mainly of B2.

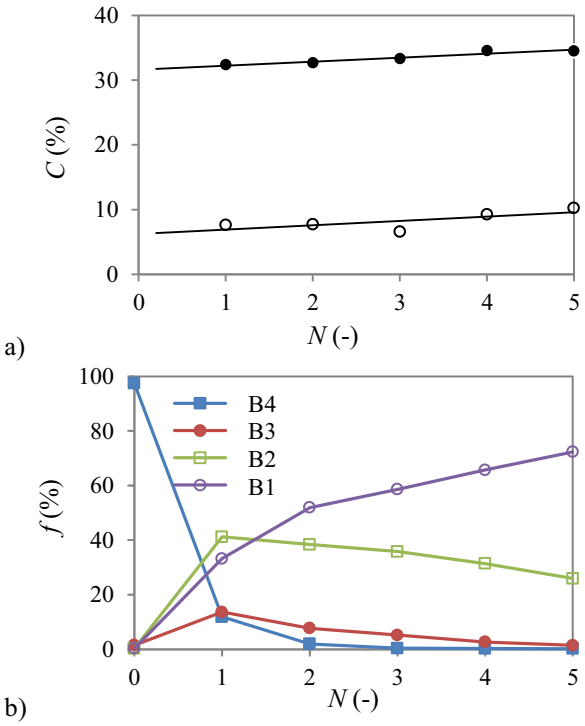

Fig. 6. Effect of pressure: multiple compressions. (a) Compressibility C; filled and empty circles with trendlines for P = 3350 and 500 kPa respectively. (b) Particle fractions f in coarse bins B1-B4. Pressure P = 3350 kPa was applied N-times.

The repeating breakage with a lower final pressure seems to be more effective than the single breakage with a larger pressure. It may be due to the particles re-arrangement at the sample handling (taking for granulometry). Particle arrangement in recompressed samples likely offers more breakable contacts and leads to higher bulk density.

The relation between the single/multiple compression is shown in the compound Fig. 7. The single compression data series (blue marks) starts at the point [L,Z] = [8,1] where we have the initially monodispersed bed. Each point is the result of a single compression experiment. As we increase the pressure P (from 0 to 5200), the data go toward lower size L and higher polydispersity Z, due to the breakage. The multiple compression data at low fixed P = 500 kPa (green marks) follow the same trend and are parametrized by the number of repetitions N. The same holds for the recompression at high fixed P = 3350 kPa (red marks). All these data behave in a similar way and have a peak in polydispersity, in the about half-size region (4 mm). The repetitive compression can be, in certain sense, equivalent to the single compression. Therefore, the existence of a possible relation between (P and N) of the former and (P) of the latter can be anticipated. The model (line) agrees qualitatively and needs some parameter adjustment to agree in values too. The difference in Z between the model and experiment shows that at the comparable stress P (Fig. 5) and average particle length L (Fig. 7), the particle size distribution is wider in the experiment than in the model. Detailed analysis revealed that this is caused by longer (unbroken) particles that survive higher loads in the experiment. A possible explanation can be that the real particles can be cracked but not separated, as seen in Fig 8. This effect is not included in the model where the crack means separation. This phenomenon needs to be studied more closely in our future work.

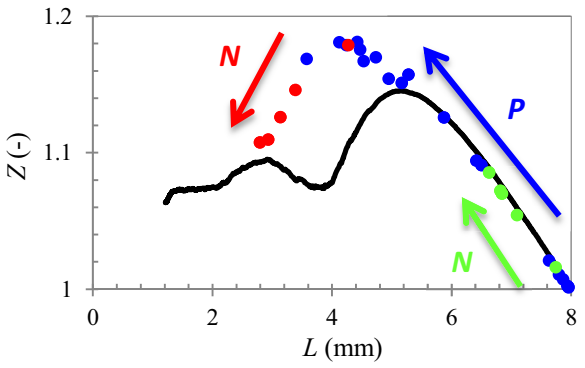

Fig. 7. Comparison of single and multiple compression. Polydispersity Z plotted vs particle average length L. Single compression with P growing from 0 to 5200 kPa (blue marks, arrow = increase). Recompression at low (500 kPa) and high (3350 kPa), fixed P with increasing N (green and red marks). Model - line.

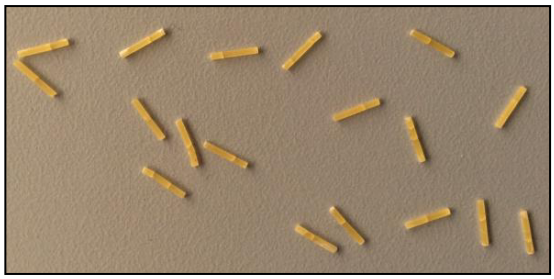

Fig. 8. Demonstration of cracks in experimental particles.

4 Conclusions

Under given conditions, the rate of compression was not the main factor of the breakage dynamics. The bed volume showed very weak effect with no obvious trend. The applied pressure determines the breakage result to a high degree. The relation between the repetitive and single compression is open for further investigation. The DEM modelling proves promising for simulating the granular media breakage.

The support by Czech Science Foundation GACR through contract No. 15-05534S is gratefully acknowledged.

5 Nomenclature

C : compressibility [%]
D : diameter of cell [m]
f : fraction of particles [%]
H : height of layer [m]
L : particles average length [m]
l : length of a particle [m]
N : number of repetition [-]
P : applied pressure [Pa]
v : piston speed [m/s]
V : initial volume of granular bed [m^3]
Z : polydispersity [-]
μ : moment

References

1. D. Schulze., *Powders and bulk solids* (Springer, Berlin, 2008)
2. H.G. Merkus., G.M.H. Meesters, (Eds.), *Production, handling and characterization of particulate materials* (Springer Cham, Switzerland, 2016)
3. H. Kalman, KONA Powder Part. J. **18** (2000)
4. Z. Grof, F. Stepanek, Phys. Rev. E **88** (2013)
5. J.F. Favier, M.H. Abbaspour-Fard, M. Kremmer, A.O. Raji, Eng. Comput. **16** (1999)
6. Z. Grof, F. Stepanek, Adv. Powder Technol. **27** (2016)